Heat Transfer Measurements Using Liquid Crystals in a Preswirl Rotating-Disk System

Gary D. Lock
Youyou Yan[1]
Paul J. Newton
Michael Wilson
J. Michael Owen

Department of Mechanical Engineering,
University of Bath,
Bath BA2 7AY, UK

Preswirl nozzles are often used in gas turbines to deliver the cooling air to the turbine blades through receiver holes in a rotating disk. The distribution of the local Nusselt number, Nu, on the rotating disk is governed by three nondimensional fluid-dynamic parameters: preswirl ratio, β_p, rotational Reynolds number, Re_ϕ, and turbulent flow parameter, λ_T. A scaled model of a gas turbine rotor–stator cavity, based on the geometry of current engine designs, has been used to create appropriate flow conditions. This paper describes how a thermochromic liquid crystal, in conjunction with a stroboscopic light and digital camera, is used in a transient experiment to obtain contour maps of Nu on the rotating disk. The thermal boundary conditions for the transient technique are such that an exponential-series solution to Fourier's one-dimensional conduction equation is necessary. A method to assess the uncertainty in the measurements is discussed and these uncertainties are quantified. The experiments reveal that Nu on the rotating disk is axisymmetric except in the region of the receiver holes, where significant two-dimensional variations have been measured. At the higher coolant flow rates studied, there is a peak in heat transfer at the radius of the preswirl nozzles. The heat transfer is governed by two flow regimes: one dominated by inertial effects associated with the impinging jets from the preswirl nozzles, and another dominated by viscous effects at lower flow rates. The Nusselt number is observed to increase as either Re_ϕ or λ_T increases.
[DOI: 10.1115/1.1787509]

1 Introduction

Preswirl nozzles are often used in gas turbines to deliver the cooling air to the turbine blades, as illustrated in Fig. 1. The stationary nozzles swirl the cooling air in the direction of rotation of the turbine disk, thereby reducing the temperature of the air relative to the blades. The designer needs to know the effect of the preswirl ratio, β_p, the coolant flow rate, and the rotational speed, Ω, on the pressure drop and temperature difference between the preswirl nozzles and the receiver holes in the disk. It is also important to know the effect of these parameters on the distribution of Nusselt number, Nu, over the surface of the rotating disk.

Owen and Rogers [1] described early studies of preswirl systems, and Owen and Wilson [2] gave a brief review of more recent heat transfer research. Metzger, Bunker, and Bosch [3] were the first to apply a thermochromic liquid crystal to the case of a rotating disk with jet impingement. Karabay, Wilson, and Owen [4] carried out a combined experimental and computational study of flow in a ''cover-plate'' (rotating cavity) preswirl system. A theoretical analysis was used to show that there was an optimal value of the preswirl ratio, for which the average Nusselt number for a heated rotating disk would be a minimum. Pilbrow et al. [5] presented experimental and computational results for heat transfer in the same cover-plate system, showing that the structure of these flows is governed principally by the values of β_p, and the turbulent-flow parameter, λ_T. For a detailed discussion of the significance of λ_T, the reader is referred to Ref. [1]. The heat transfer is governed by the above two parameters as well as by the rotational Reynolds number, Re_ϕ, and by the temperature distribution on the rotating disk.

Designers can obtain some information using turbine-based rigs running close to engine-operating conditions. However, deeper insight can be gained from fundamental research that measures, computes, and explains the flow and heat transfer in generic, fully instrumented rigs operating under more benign conditions. Computational codes, validated on these detailed measurements, can then be used to conduct calculations extrapolated to engine conditions.

This paper describes a generic rig, which has been constructed to study the fluid dynamics and heat transfer in preswirl systems. The experimental facility is a simplified model of a gas turbine rotor–stator system designed to accommodate pressure and temperature instrumentation in the test section and to provide optical access to the wheel space. The fluid dynamics has been investigated both experimentally and computationally by Yan et al. [6]. The effects of rotational speed, flow rate, preswirl ratio, and the number of preswirl nozzles on the flow field and on the total pressure losses in the system have been reported. These measurements and computations showed that there was a significant loss of total pressure between the outlet from the preswirl nozzles and the rotating core of fluid in the wheel space. This loss increased as the preswirl flow rate and inlet swirl ratio increased, and as the number of nozzles decreased. The discharge coefficient of the receiver holes increased as the swirl ratio at the receiver-hole radius approached unity.

The complementary measurements of heat transfer using thermochromic liquid crystals (TLCs) are discussed here, featuring the novel technique of stroboscopic lighting and an exponential-series solution to Fourier's conduction equation. Contour maps of Nu on the rotating disk have been measured, including detailed two-dimensional patterns around the blade receiver holes. Al-

[1]Present address: City University, London, Northampton Square, London EC1V 0HB, U.K.

Contributed by the International Gas Turbine Institute (IGTI) of THE AMERICAN SOCIETY OF MECHANICAL ENGINEERS for publication in the ASME JOURNAL OF ENGINEERING FOR GAS TURBINES AND POWER. Paper presented at the International Gas Turbine and Aeroengine Congress and Exhibition, Atlanta, GA, June 16–19, 2003, Paper No. 2003-GT-38123. Manuscript received by IGTI, October 2002, final revision, March 2003. Associate Editor: H. R. Simmons.

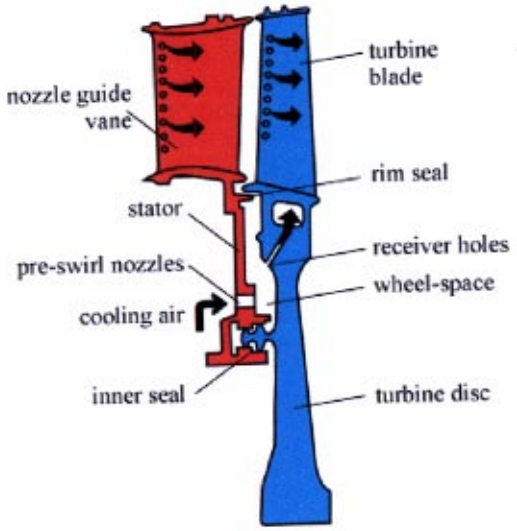

Fig. 1 Simplified diagram of typical preswirl cooling-air system for a gas turbine

though some authors have measured the radial distribution of Nu, there are no published records of contour maps over the disk surface.

2 Experimental Apparatus and Instrumentation

2.1 Apparatus. Experiments were conducted using a scaled model of a gas-turbine rotor–stator system. The geometry, which was based on information obtained for existing engine designs, is illustrated schematically in Fig. 2. The air entered the test section through the stator at low radius via preswirl nozzles and flowed radially outward between the rotating disk and the stator, exiting through receiver holes in the rotating disk representing the entrance to the blade-cooling passages in the engine.

The disk radius was $b=216$ mm, and the other principal dimensions are the inner-to-outer radius ratio $a/b=0.67$ and the gap ratio $s/b=0.051$. The stator was machined from aluminum, and contained 24 circular preswirl nozzles angled at 20 deg to the tangential direction. The rotating disk was machined from transparent polycarbonate, with sectors sprayed with TLC and black paint, and contained 60 axial receiver holes with a length-to-diameter ratio of 1.25. The nondimensional radius of the nozzles, $x_p=r_p/b=0.74$, was less than that of the receiver holes, $x_b=r_b/b=0.93$, and the area ratio of the receiver holes to that of the nozzles is 2.9.

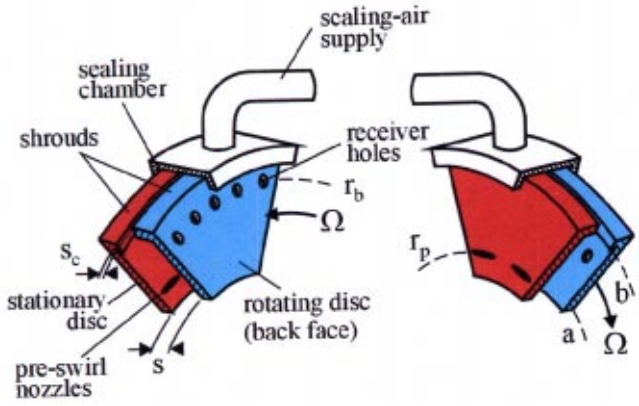

Fig. 2 Schematic diagram of test-section geometry

The outer shroud has two sections, one attached to the stator and the other the rotor, which were separated by an axial clearance, s_c. The inner seal, not shown in Fig. 2, was stationary. A stationary, annular "sealing chamber" was fitted around the periphery of the cavity, and the chamber was pressurised by a separate flow to form a labyrinth seal. Some of the preswirl air was allowed to leak past the labyrinth seal, and this leakage flow rate was controlled by the air supplied to the seal. It was therefore possible to control independently the mass flow rates of the preswirl, blade cooling, and sealing flows. These mass flow rates were chosen to simulate engine-representative values of β_p and λ_T.

The disk could be rotated up to speeds of 5000 rpm, providing a maximum rotational Reynolds numbers, Re_ϕ (based on disk radius) up to 1.2×10^6. This value is typically an order of magnitude less than those found in gas turbines. However, as discussed above, the flow structure within the rotating cavity depends principally on β_p and λ_T and only weakly on Re_ϕ. Hence the flow structure is considered to be representative of that found in cooling systems of engines. Nusselt numbers were measured for around 20 test conditions covering the following parametric range: $0.78\times10^6<\mathrm{Re}_\phi<1.2\times10^6$; $0.125<\lambda_T<0.36$; $0.5<\beta_p<1.5$.

2.2 Instrumentation. A total-temperature probe and pitot tube located in the outlet of the nozzles, together with a static-pressure tap between the nozzles, were used to measure the total and static temperature and the velocity of the inlet flow. Static pressure taps were located at nine radial stations in the stator, and nine pitot tubes were located at the same radii in the midaxial plane of the wheel space. This enabled the measurement of the radial distribution of static and total pressure, and of V_ϕ, the tangential velocity of the air in the core outside the boundary layers. As the "blade-cooling air" discharged directly to atmosphere, it was also possible to measure the discharge coefficient of the receiver holes. Measurements of the fluid dynamics of the experimental facility are presented by Yan et al. [6].

Local heat transfer coefficients on the rotating disk were determined from surface-temperature measurements using TLCs. The experiments, which were transient and conducted under known thermal boundary conditions, relied on the accurate measurement of the time taken for the narrow-band TLCs on the rotor surface to reach a unique value of hue, which had been calibrated against temperature. The crystals were sprayed on the disk in sectors inside the wheel space, which could be viewed through the transparent polycarbonate by a digital video camera, running at 25 frames per second, under the illumination of a strobe light synchronized to the disk frequency. A thin layer of black paint was used to provide contrast to the color play of the TLC. The in situ calibration of the TLC is discussed in the next section, though it should be noted that the hue was measured as a function of temperature over a range of strobe frequencies corresponding to rotational disk speeds up to 5000 rpm. The strobe had a flash duration of less than 8 μs which, at 5000 rpm, corresponded to 0.24 deg angular rotation of the disk.

Figure 3 is a schematic diagram illustrating the arrangement of pipes providing the air flow to the test section, where all mass flow rates were measured using orifice plates designed to British Standards (BS1042). A mesh heater, designed using the method of Gillespie, Wang, and Ireland [7], was used to generate a sudden change in the air temperature and to create a well-controlled thermal boundary condition for the transient experiments. The mesh was made of 90-μm-diam stainless-steel wire with an open area of 38% and overall dimensions of 60×120 mm. The mesh was soldered to bus bars, and the additional support of three strengthening rods of 3 mm diameter was required due to the pressure drop across the mesh. A welding unit and control box provided a current of typically 150 A, which increased the air temperature across the mesh heater by 40°C (with a standard deviation of 0.2°C) for a mass flow rate of 0.1 kg/s. All pipework downstream of the

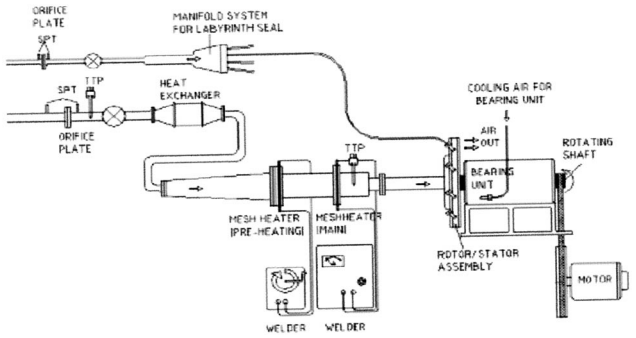

Fig. 3 Schematic layout of experiment

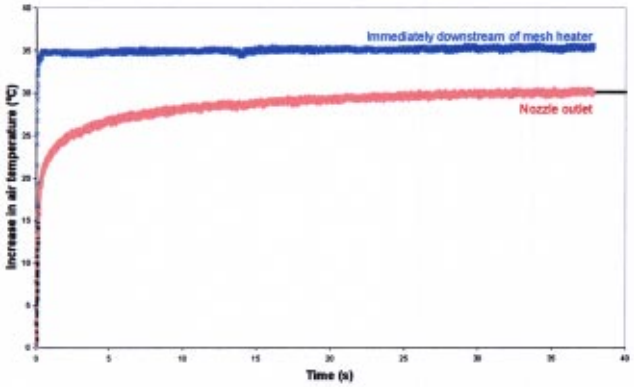

Fig. 4 Increase in air temperature with time measured at two locations; a fitted curve is also shown for $m=3$

mesh heater was thermally insulated using low-conductivity Rhoacell, a closed-pore structural foam with low thermal conductivity. This pipework had three main components: a 350-mm length of rectangular cross section, a 350-mm length of circular cross section, and a radial diffuser; there was also a short entry length into the preswirl nozzles. The temperature history of the air leaving the preswirl nozzles is described in Sec. 3.

Before the main mesh heater was switched on, the apparatus was left running, at the required speed and flow rate, to enable it to reach thermal equilibrium. When the air from the compressor was not equal to the ambient temperature in the laboratory, it was either cooled by a heat exchanger or heated by a second mesh heater upstream of the main heater. In practice, it was not possible to achieve perfect thermal equilibrium, and there was always a small temperature difference between the rotating disk and the air, as discussed in Sec. 4.

3 Temperature Measurement

3.1 Total-Temperature Probes. A conventional total-temperature probe usually contains a thermocouple, the bead of which is located inside a stainless-steel tube. Such probes have a large recovery factor ($\approx$0.95) but a poor time response. For the tests described here, a K-type bare-wire thermocouple, made from wires of 25 μm diameter, was constructed. The wires were contained inside a stainless steel tube with the bead outside; there was a distance of 3.5 mm (or 140 wire diameters) between the exposed bead and the tip of the tube. This construction method supported the thermocouple wires but reduced the thermal error resulting from transient conduction from the bead to the tube. The result was a robust probe with a time constant of less than 40 ms. A consistent probe recovery factor of 0.78 was measured over a range of air speeds up to 120 m/s.

Figure 4 shows a typical increase in air temperature with time measured by the probe immediately downstream of the mesh heater and at the outlet of the preswirl nozzles. Downstream of the heater there is a good approximation to a step change. Owing to the thermal inertia of the ducting between the heater and the test section, a step change is not produced at the nozzles; it can be seen that a good fit to the temperature is provided by an exponential series of $m=3$ terms (see Sec. 4.2). It seems likely that three terms are required in the exponential fit because there are three distinct geometric sections to the duct downstream of the heater mesh, as discussed above. Typically the TLC color-change times on the disk surface ranged between 1 and 20 s (depending on the local heat transfer coefficient), and these times are of similar magnitude to the time constants of the exponential rise in air temperature.

3.2 Calibration of TLCs. Microencapsulated TLCs were purchased commercially in the form of a water-based slurry. Three types of TLC were used: two narrow-band crystals optically active over a temperature range of around 1°C near 30°C (R30C1W) and 40°C (R40C1W), and one wide-band crystal (R18C20W) active from approximately 18°C over a 20°C range.

The crystals were calibrated against temperature by recording the red, green, and blue (RGB) signals of light reflected from the TLC, under known temperature and illumination, using a digital camera, an isothermal copper block, and an AGEMA 870C infrared-imager [8]. The RGB signals were converted into hues, which increase monotonically with temperature.

The TLC was applied to the rotor surface using an airbrush, and black paint was sprayed on top of the TLC to provide contrast to the color play from the crystals. The overall thickness (TLC and paint) was approximately 25 μm. During the experiments the TLC was viewed through the transparent polycarbonate disk using the stroboscopic light synchronized to the rotational speed of the disk. For the calibration, the stator was removed to gain direct optical access to the front surface of the disk, which was coated in TLC under black paint and heated quasiaxisymmetrically by a jet of hot air. The surface temperature of the front face was measured using an infrared imager. The back face of the disk was simultaneously illuminated by the stroboscopic light and the TLC was viewed by the digital camera, located behind the disk. The locations of the stroboscopic light and camera were the same as those used in the experiments, creating an in situ calibration.

It has been shown [8,9] that rotational speed has no significant effect on the calibration of TLCs, and so the calibrations were conducted with the disk stationary. To ensure that the strobe frequency had no effect, calibrations were carried out for frequencies corresponding to 3000, 4000, and 5000 rpm.

Figure 5 shows the calibrated variation of temperature with

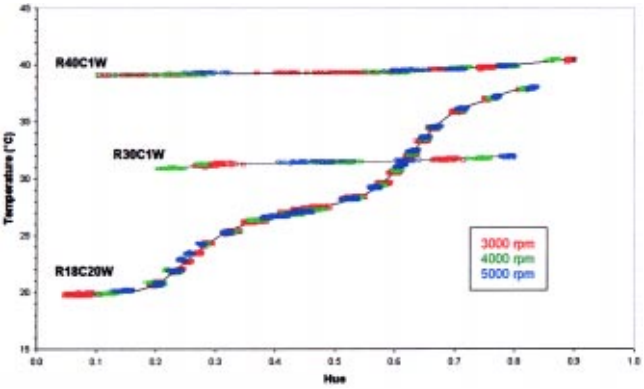

Fig. 5 Calibrated temperature versus normalized hue for three crystals at three strobe frequencies

normalized hues for all three crystals. The hue changed from 0 to 1 as the TLC changed color from red through green to blue as it was activated through its transition temperature. In all cases, the effect of the strobe frequency is insignificant. The estimated random uncertainties are ±1°C for the wide-band and ±0.1°C for the narrow-band crystals.

4 Analysis of Experimental Data

This section presents a technique for determining the convective heat transfer coefficient, h, for transient experiments where the air temperature, which is used as a boundary condition for Fourier's one-dimensional conduction equation, is represented by an exponential series.

4.1 Definition of the Heat Transfer Coefficient. Before proceeding, it is convenient to define h as

$$q_w = h(T_{aw} - T_w), \tag{4.1}$$

where q_w is the surface heat flux from the air to the wall, T_w is the surface temperature of the wall, and T_{aw} is the adiabatic-wall temperature. T_{aw} depends on the total-temperature of the air, T_a, and on the fluid dynamics. For example, for boundary layer flow over a flat plate,

$$T_{aw} = T_a - (1-R)\frac{U^2}{2c_p}, \tag{4.2}$$

where U is the free stream velocity and R is the recovery factor. For the case where U is invariant with time, Eq. (4.2) can be expressed as

$$T_{aw} = T_a + F, \tag{4.3}$$

where F is a time-invariant term. In general, F depends on the flow, but for the above case, $F=(R-1)U^2/2c_p$.

4.2 Solution of Fourier's Equation. In a typical transient test, a step change in air temperature is generated, and a narrow-band TLC is used to determine the surface temperature, T_w, of the test piece. Knowing the time, t, at which the surface reaches T_w, h (assumed time-invariant) can be calculated from the solution of Fourier's one-dimensional conduction equation for the case of a semi-infinite plate subjected to a step change in air temperature.

In the tests described here, the mesh heater created an effective step change in the air temperature, but at the test section an exponential type of behavior (or so-called "slow transient") was produced, as shown in Fig. 4. The air temperature, T_a, could be fitted by an exponential series of m terms, such that

$$T_a(t) = T_{a,0} + \sum_{j=1}^{m} T_{a,j}(1 - e^{-t/\tau_j}), \tag{4.4}$$

where $T_{a,0}$ is the air temperature at $t=0$, and $T_{a,j}$ and τ_j are the constant amplitudes and time constants, respectively.

The adiabatic wall temperature can be written as

$$T_{aw}(t) = T_a(t) + F, \tag{4.5}$$

where F is a time-invariant parameter that depends on the flow. As $t \to \infty$,

$$T_{aw,\infty} = T_0 + \sum_{j=1}^{m} T_{a,j} \tag{4.6}$$

where T_0 is the initial temperature of the wall, such that

$$T_0 = T_{a,0} + F. \tag{4.7}$$

Fourier's conduction equation for a semi-infinite slab has been solved by Gillespie, Wang, and Ireland [10] for the case where there is a simple exponential increase in the air temperature, corresponding to the case where $m=1$ in Eq. (4.4). The solution is

$$\Theta = \frac{T_w - T_0}{T_{aw,\infty} - T_0} = g(\beta, \beta_\tau), \tag{4.8}$$

where

$$g(\beta,\beta_\tau) = 1 - \frac{1}{1+\beta_\tau^2} e^{\beta^2}\,\mathrm{erfc}(\beta) - e^{-t/\tau}\frac{\beta_\tau^2}{1+\beta_\tau^2} \times \left\{ 1 + \frac{1}{\beta_\tau}\left[\frac{1}{\pi}\sqrt{\frac{t}{\tau}} + \frac{2}{\pi}\sum_{n=1}^{\infty} \frac{1}{n} e^{-n^2/4} \sinh\left(n\sqrt{\frac{t}{\tau}} \right) \right] \right\}, \tag{4.9}$$

$$\beta = \frac{h\sqrt{t}}{\sqrt{\rho c k}}, \tag{4.10}$$

and

$$\beta_\tau = \frac{h\sqrt{\tau}}{\sqrt{\rho c k}}. \tag{4.11}$$

For the case where $\tau=0$, Eq. (4.8) simplifies to

$$\Theta = f(\beta), \tag{4.12}$$

where

$$f(\beta) = 1 - e^{\beta^2}\,\mathrm{erfc}(\beta), \tag{4.13}$$

which is the well-known solution of Fourier's equation for a step change in the air temperature.

The general solution for an exponential series, corresponding to Eq. (4.6), is given by Newton et al. [11] as

$$\Theta = \sum_{j=1}^{m} \frac{T_{a,j}}{T_{aw,\infty} - T_0} g(\beta, \beta_{\tau_j}). \tag{4.14}$$

For the special case where $m=1$, $T_{a,1} = T_{aw,\infty} - T_0$ and Eq. (4.14) reduces to Eq. (4.8).

4.3 Data Analysis. The experimental data were analyzed by making a least-squares fit of an exponential series (Eq. (4.4)) to the measured variation of air temperature with time. This enabled $T_{aw,\infty}$ and $T_{a,j}$ to be calculated for $j=1$ to m; a value of $m=3$ was found to give an acceptable fit in all cases tested.

The initial wall temperature, T_0, was determined using Eq. (4.7) with measured values of $T_{a,0}$ and a theoretical value of F. The value of T_0 found in this way was similar to, but considered to be more accurate than, the value obtained using wide-band TLCs (see Ref. [11]). The value of T_w was determined from an appropriate narrow-band crystal. With knowledge of T_w, T_0, and $T_{aw,\infty}$, Θ was calculated, and h was obtained from the numerical solution of Eq. (4.14).

An alternative procedure for experiments featuring a slow transient is to use a wide-band TLC (with a transition temperature range of, say, 20°C) to measure the complete variation of surface temperature with time. By use of Duhamel's method, Fourier's solution can be solved and h determined. However, the uncertainty in measurement of surface temperature using wide-band TLCs is generally much greater than that using narrow-band TLCs, and this results in a large uncertainty in h [12,13]. The advantage of the analysis presented here is that, just as for the step-change case, which is the limit of the exponential-series solution, it is not necessary to know the wall-temperature history: only a single narrow-band TLC is needed to determine h. This allows the accuracy of the simple step-change method to be brought to the more difficult case of the slow transient. A typical case is discussed below.

5 Typical Test Case

Figures 6(*a*) to 6(*d*) are raw color images selected from a time sequence obtained by the digital camera (operating at 25 frames

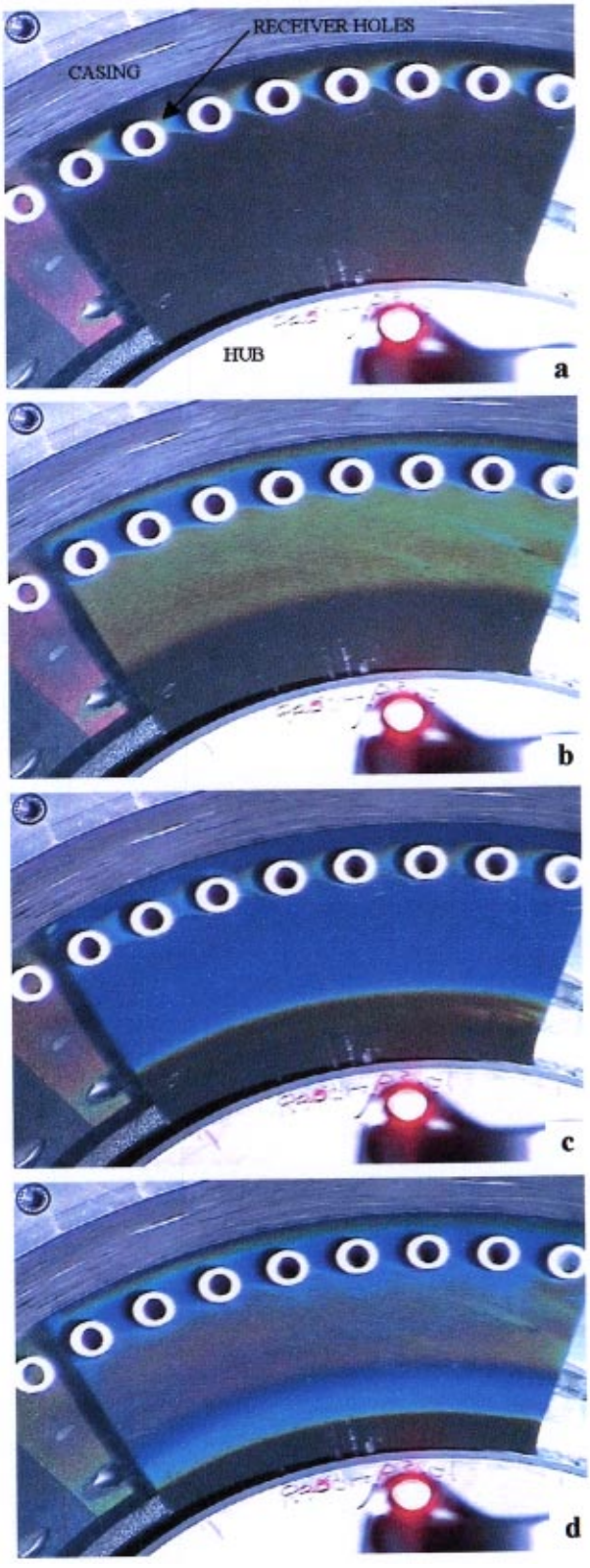

Fig. 6 ***a–d*** **(top to bottom) Video recordings of disk surface showing change of color of TLC with time**

per second) during a typical experiment. These images show the color play of the TLC as viewed through the transparent polycarbonate disk. Initially clear when below its activation temperature, the TLC changed color from red to green to blue as the disk was

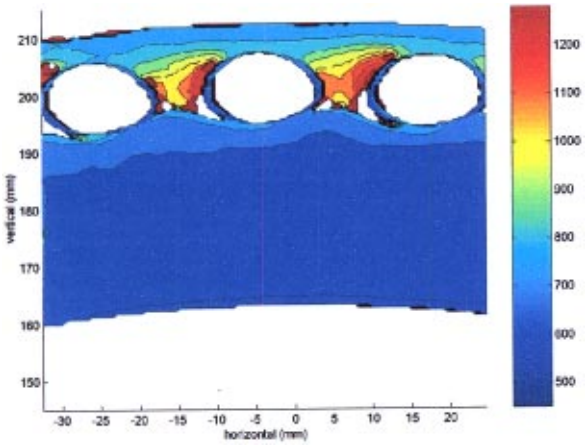

Fig. 7 Contours of Nu: $Re_\phi \approx 0.8\times10^6$, $\lambda_T \approx 0.125$, $\beta_p \approx 0.5$; the disk is rotating clockwise

heated by the hot gas entering through the preswirl nozzles. The images appear ''frozen'' because the rotor was illuminated by the stroboscopic light synchronized with the disk rotating at 5000 rpm.

A color version of Fig. 6 (and Figs. 7 and 8) appear in ASME paper GT-2003-38123. The hub and casing, at radii *a* and *b*, are marked in Fig. 6(*a*). The blade receiver holes, insulated using low-conductivity, white-colored Rhoacell foam, are also labeled. The narrow-band TLC and overcoat of black paint had been sprayed in a 48 deg sector on the disk covering 8 of the 60 receiver holes. To the left of this painted sector the stator, coated with a wide-band (initially red) TLC, and two of the 24 preswirl nozzles are visible through the transparent (unpainted) polycarbonate at low radius. Some shadows appear around the receiver holes due to constraints with the lighting and viewing angles.

In Fig. 6(*a*) the 30°C narrow-band TLC has been activated into its visible range (shown as blue) near the blade receiver holes. Elsewhere on the disk the TLC is still clear (showing black), indicating that there is a region of relatively high heat transfer around the holes. The virtually identical TLC patterns around each of the receiver holes clearly indicate the excellent periodicity of the flow structure. In Figs. 6(*b*) and 6(*c*), the 30°C crystal has been activated (green and blue, respectively) at radii between the preswirl nozzles and the receiver holes. In Fig. 6(*c*) the 40°C TLC has been activated by temperature (light blue) in the region around the receiver holes and has turned dark blue in Fig. 6(*d*). The 40°C TLC is activated at lower radii in Fig. 6(*d*) (red-green). Note that the stator, as indicated by the change in color of the wide-band TLC, has also been heated throughout this transient process.

These RGB images (of 800×600 pixels), recorded at 25 frames per second by the digital camera, were subsequently converted to hues on a PC. It was then possible to obtain the hue history of each pixel in the image and hence the time taken for the surface to reach a prescribed value of hue. Thus the time taken for the surface to reach the temperature of the calibrated narrow-band crystal, T_w, from an initial temperature, T_0, was measured at each pixel on the active surface of the disk in the field-of-view of the camera. A ''median filter,'' using the median of nine adjacent pixels, was used to reduce the uncertainty in the measured values of T_w.

6 Nusselt Number

Figure 7 shows contours of the measured Nusselt number on the rotating disk for $Re_\phi = 0.8\times10^6$, $\lambda_T \approx 0.125$, and $\beta_p \approx 0.5$; the direction of rotation of the disk is clockwise. The distribution of Nu is largely axisymmetric, except in the region around the re-

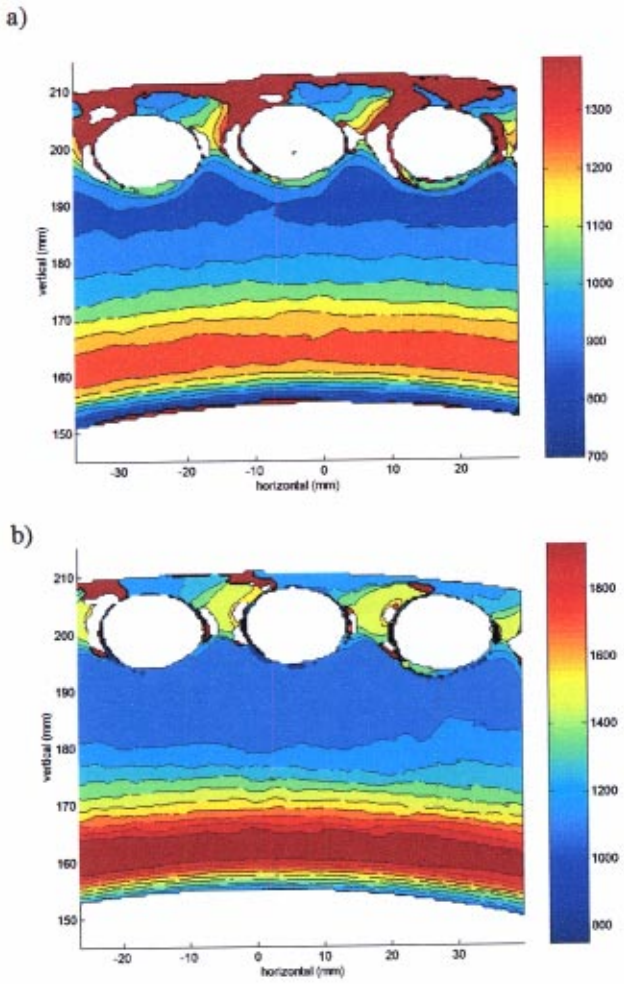

Fig. 8 Effect of Re_ϕ on contours Nu for $\lambda_T \approx 0.36$ and $\beta_p \approx 1.4$: (*a*) $Re_\phi \approx 0.8\times10^6$, (*b*) $Re_\phi \approx 1.18\times10^6$; the disk is rotating clockwise

ceiver holes. The highest heat transfer rates occur between the holes, and there is repeatability in both magnitudes and the variations of Nu between successive holes.

Figures 8(*a*) and 8(*b*) show contours of Nu for a higher flow rate, $\lambda_T \approx 0.36$, $\beta_p \approx 1.4$, for $Re_\phi = 0.8\times10^6$ and $Re_\phi = 1.18\times10^6$, respectively. The color scales have been chosen independently in order to show clearly the variations around the receiver holes. Comparing Fig. 4 and Fig. 5(*a*), for which $Re_\phi = 0.8\times10^6$ in both cases, there is higher heat transfer around the preswirl nozzle radius, $x_p = 0.74$, at the higher flow rate. There are similar variations (and similarly good repeatability of results) between the receiver holes on the disk; Nu is also higher in this region for the higher flow rate case. Figures 8(*a*) and 8(*b*) show that Nu increases generally with increasing Re_ϕ.

6.1 Effect of Re_ϕ on Radial Variation of Nu. The variations of Nu with the parameters λ_T and β_p, and with Re_ϕ, are best observed by using results taken along a radial line midway between receiver holes. Figure 9 shows the effect of Re_ϕ on the measured radial variation of Nusselt number at two fixed values of λ_T (0.125 and 0.36 approximately), for which $\beta_p \approx 0.5$ and 1.4, respectively. For each fixed value of λ_T (and β_p), the magnitude of Nu increases with increasing Re_ϕ, but there is little effect of Re_ϕ on the *shape* of the Nu distributions. For all cases, there is a peak in measured values of Nu in the region near the receiver holes on the disk. Figure 9(*a*) ($\lambda_T \approx 0.125$, $\beta_p \approx 0.5$) shows that Nu increases with radius between the preswirl nozzle radius, x_p

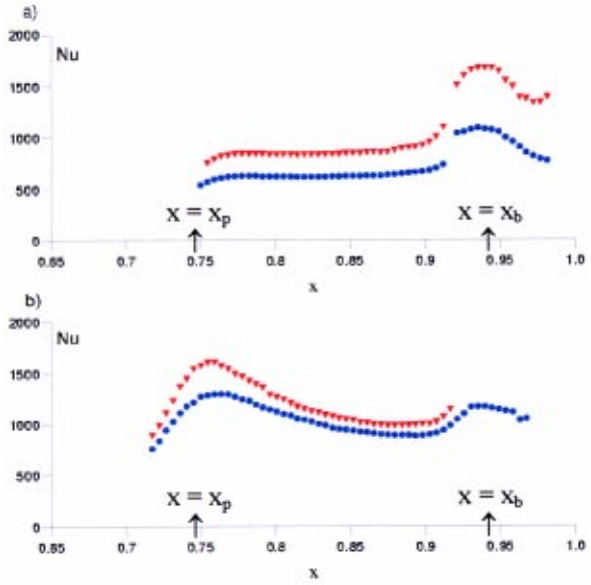

Fig. 9 Effect of Re_ϕ on radial variation of Nu (*a*) $\lambda_T \approx 0.125$, $\beta_p \approx 0.52$; (*b*) $\lambda_T \approx 0.36$, $\beta_p \approx 1.4$ $Re_\phi \approx 0.8\times10^6$ ● $Re_\phi \approx 1.2\times10^6$ ▼

$= 0.74$, and the receiver holes. This behavior is similar, qualitatively, to heat transfer in a simple rotor–stator system with a radial outflow [14], suggesting that heat transfer is controlled mainly by the boundary-layer flow on the rotating disk. For $x > 0.9$, there is a rapid rise in measured Nu. In this region, disk boundary layer fluid enters the receiver holes and there is strong flow axially toward the disk, causing an increase in heat transfer.

Figure 9*b* shows that for $\lambda_T \approx 0.36$ ($\beta_p \approx 1.4$) a local peak in Nu occurs around the nozzle radius x_p, and Nu decreases for $x_p < x < x_b$. This suggests that inertial ''impingement'' effects have a more significant influence, due to the more powerful preswirl flow at this higher value of λ_T, than for the cases in Fig. 9(*a*).

6.2 Effect of λ_T and β_p on the Radial Variation of Nu. Figures 9(*a*) and 9(*b*) also show, respectively, the effect of varying λ_T (and, as a consequence, varying β_p) on the measured radial variation of Nu for $Re_\phi \approx 0.8\times10^6$ (blue circles) and 1.2×10^6 (red triangles). At both values of Re_ϕ, there is a similar transition in the variation of Nu with x, from the viscous behavior described above for $\lambda_T \approx 0.125$ ($\beta_p \approx 0.5$) to inertial behavior for $\lambda_T \approx 0.36$ ($\beta_p \approx 1.4$).

The combined effect of increasing λ_T and β_p at fixed Re_ϕ is greatest for $x < 0.9$, approximately. There is less sensitivity to λ_T and β_p for the region around and outward of the receiver holes, and this sensitivity also tends to decrease as Re_ϕ increases.

6.3 Use of Two Crystals. The method of analysis described in Sec. 4 only requires a measurement of a single narrow-band TLC. Two narrow-band TLCs were used to test the accuracy of the measurements. Figure 10 shows *h*, rather than Nu, again measured along a radius midway between two receiver holes for the viscous and inertial cases discussed above. Data from both the 30 and 40°C TLCs are shown.

There is good agreement between the data collected from the two TLCs for the viscous case. However, in the inertial case, *h* measured using the 40°C crystal is consistently higher than that obtained using the 30°C crystal. These cases are typical examples from a range of experimental data. Before discussing possible reasons for differences in the measurements of *h*, it is necessary to consider the uncertainties in these measurements.

The uncertainty analysis described by Owen, Newton, and Lock [13] was used to create the ''uncertainty bars'' shown in Fig. 10. Small, random uncertainties in the measured temperature can produce large uncertainties in the calculated values of *h*. If P_{T_w}, P_{T_0},

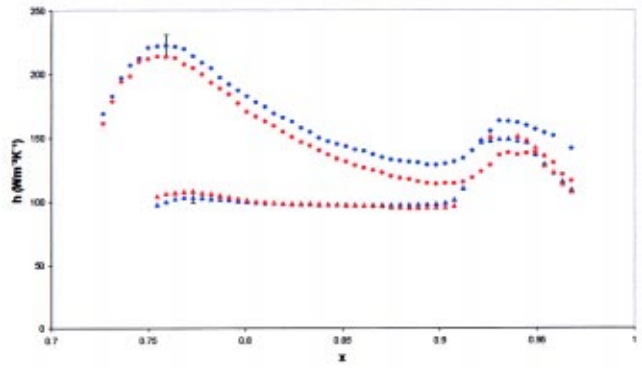

Fig. 10 Heat transfer coefficient versus normalized radius for viscous and inertial flows. ▲ Viscous—H40; ● Inertial—H40; ▲ Viscous—H30; ● Inertial—H30. (*h* uncertainty for 0.2°C temperature uncertainty.)

and $P_{T_{aw}}$ are the relative uncertainties (95% confidence estimates) in T_w, T_0 and T_{aw}, respectively, then P_h, the relative uncertainty in h, can be determined from

$$\frac{P_h}{h} = \Phi_h \frac{P_T}{T_{aw} - T_0}, \tag{6.1}$$

where Φ_h is the so-called *amplification parameter* and $P_T = \max(P_{T_w}, P_{T_0}, P_{T_{aw}})$.

The uncertainty bars in Fig. 10 are based on a 0.2°C temperature uncertainty. Despite the random uncertainties, there is no evidence of significant scatter in the results. The ''smoothness'' of the distribution of h is attributed to the smoothing of the air temperature and to the median filtering used for the wall temperatures.

There are three suspected reasons for the differences in the measurements of h from the two crystals: (i) incorrect values of T_{aw}; (ii) incorrect values of T_0; (iii) effect of radial distribution of T_w.

(i) T_{aw}, given by Eq. (4.5), depends on T_a, the local temperature in the fluid core. Unfortunately this temperature was not measured in the experiments but was assumed to be equal to the measured temperature at exit from the preswirl nozzles. It is speculated that, as heat flows from the air to the rotating disk, the temperature of the fluid in the core, and hence T_{aw}, will be less than T_a. Consequently the value of T_{aw} given by Eq. (4.2) will overestimate the true value, which in turn would cause an underestimate in the true value of h. The values of h calculated from the 40°C crystal should, by this argument, be closer to the true values than those from the 30°C crystal. This uncertainty in T_a would have a more significant in the inertial regime than the viscous regime; in the former there is relatively high heat transfer and more mixing of air between the core and the region near the wall.

(ii) There is an uncertainty in the value of T_0 and this could bias the calculated values of h. A bias in T_0 would qualitatively affect both measurements of h in the same way, though not in a quantitatively equal manner.

(iii) As discussed by Butler and Baughn [15], the distribution of h is affected by the distribution of T_w. This effect is particularly significant in rotating-disk systems [1] where the radial distribution of h depends strongly on the radial gradient of disk temperature. As the radial distributions of T_w are, perforce, different for the two crystals, it is reasonable to speculate that the radial distribution of h will be different. In addition, in regions of high local temperature gradients there is an effect of lateral conduction which can cause an overestimate in the value of h from one-dimensional conduction analysis [16]. This error has not been quantified here.

The fact that differences in h, albeit within the limits of experimental uncertainty, could be measured is a tribute to the exponential-series technique and to the careful calibration of the TLCs. These measurements also reveal the benefits of using two crystals to evaluate h: one crystal would only provide the bliss of ignorance!

The measurements of h obtained using the 40°C crystal are considered more accurate than those obtained using the 30°C crystal. All data in Figs. 7–9 are based on the 40°C crystal.

7 Conclusions

An experimental facility has been built to investigate the heat transfer and fluid dynamics of a rotor–stator system with preswirled air under engine-representative flow structure. The facility has been designed to accommodate pressure and temperature instrumentation in the test section and to provide optical access to the wheel space.

A thermochromic liquid crystal (TLC), in conjunction with a stroboscopic light and digital video camera, has been used to obtain contour maps of the Nusselt number, Nu, on the rotating disk. Both wide-band and narrow-band TLCs were used and carefully calibrated *in situ* using an infrared imager.

A mesh heater was used to generate an air temperature history in the test section, which was represented as an exponential series of three terms. An analysis has been developed to determine values of Nu by using this series as a boundary condition for Fourier's one-dimensional conduction equation. This technique has the advantage, in terms of accuracy and simplicity, that only a single narrow-band TLC is needed to determine h.

Two heat transfer regimes were observed experimentally: a viscous regime at relatively low values of λ_T, and an inertial regime at high values of λ_T. The viscous regime corresponds to axisymmetric boundary layer flow over most of the rotating disk: for $x < x_b$, Nu increases as x increases. Three-dimensional flow near the receiver holes on the disk, at $x = x_b$, creates nonaxisymmetric flow in this region, with large values of Nu between and around the holes. The inertial regime corresponds to impingement on the rotating disk around the preswirl nozzle radius, $x = x_p$. There is a peak in Nu near $x = x_p$ and, for $x_p < x < x_b$, Nu decreases as x increases; this behavior is also virtually axisymmetric. As for the viscous regime, there are large values and two-dimensional variations of Nu around the receiver holes. For both regimes, Nu increases as Re_ϕ, λ_T, and β_p increase.

Acknowledgment

This work was funded by Alstom Power, Ltd. and the U.K. EPSRC.

Nomenclature

a = inner radius of the disk
b = outer radius of the disk
c = specific heat of wall
c_p = specific heat at constant pressure of air
C_w = nondimensional mass flow rate ($= \dot{m}/\mu b$)
$f(\beta)$ = step-change solution of Fourier's equation
F = time-invariant adiabatic-wall parameter ($= T_{aw} - T_a$)
$g(\beta, \beta_\tau)$ = exponential solution of Fourier's equation
h = heat transfer coefficient [$= q_w/(T_{aw} - T_w)$]
k = thermal conductivity of wall
m = number of terms in exponential series
Nu = Nusselt number [$= q_w r/k(T_{aw} - T_w)$]
P = uncertainty in measured value
q_w = heat flux from air to wall
r = radius from axis of rotation
R = recovery factor
Re_ϕ = rotational Reynolds number ($= \rho \Omega b^2/\mu$)
s = gap width
s_c = clearance spacing
t = time
T = temperature inside wall

T_a = total temperature of air
T_{aw} = adiabatic-wall temperature
T_w = surface temperature of wall
U = free-stream velocity
V_ϕ = tangential component of velocity
x = nondimensional radius ($=r/b$)
α = thermal diffusivity of wall ($=k/\rho c$)
β = parameter in step-change solution ($=h\sqrt{t/\rho ck}$)
β_p = preswirl ratio ($=V_{\phi,p}/\Omega r_p$)
β_τ = parameter in exponential solution ($=h\sqrt{\tau/\rho ck}$)
λ_T = turbulent flow parameter ($=C_{w,p}/\mathrm{Re}_\phi^{0.8}$)
ρ = density
Θ = nondimensional temperature [$=(T_w-T_0)/(T_{aw,\infty}-T_0)$]
Φ = amplification parameter for uncertainties
μ = dynamic viscosity
Ω = angular speed of rotating disk
τ = time constant

Subscripts

h = with reference to heat transfer coefficient
j = jth term in series
T = with reference to maximum value of P_{T_w}, P_{T_0}, and $P_{T_{aw}}$
T_{aw} = with reference to adiabatic wall temperature
T_0 = with reference to initial temperature
T_w = with reference to surface temperature
p = preswirl nozzle
0 = value at $t=0$
∞ = value as $t\to\infty$

References

[1] Owen, J. M., and Rogers, R. H., 1989, *Flow and Heat Transfer in Rotating Disc Systems*: Vol. 1, *Rotor-Stator Systems*, Research Studies Press, Taunton, UK and Wiley, NY.

[2] Owen, J. M., and Wilson, M., 2000, "Some Current Research in Rotating-Disc Systems," in Turbine 2000 Int. Symp. on Heat Transfer in Gas Turbine Systems, Turkey, August 13–18, in Heat Transfer in Gas Turbine Systems, Annals of the New York Academy of Sciences, **934**, pp. 206–221.

[3] Metzger, D. E., Bunker, R. S., and Bosch, G., 1991, "Transient Liquid Crystal Measurement of Local Heat Transfer on a Rotating Disk With Jet Impingement," ASME J. Turbomach., **113**, pp. 52–59.

[4] Karabay, H., Wilson, M., and Owen, J. M., 2001, "Predictions of Effect of Swirl on Flow and Heat Transfer in a Rotating Cavity," Int. J. Heat Fluid Flow, **22**, pp. 143–155.

[5] Pilbrow, R., Karabay, H., Wilson, M., and Owen, J. M., 1999, "Heat Transfer in a 'Cover-Plate' Pre-Swirl Rotating-Disc System," ASME J. Turbomach., **121**, pp. 249–256.

[6] Yan, Y., Gord, M. F., Lock, G. D., Wilson, M., and Owen, J. M., 2002, Fluid dynamics of a pre-swirl rotating-disk system, ASME paper 2002-GT-30415 (to be published in the J Turbomachinery).

[7] Gillespie, D. R. H., Wang, Z., and Ireland, P. T., 2001, Heater element, European Patent No. 0847679.

[8] Syson, B. J., Pilbrow, R. G., and Owen, J. M., 1996, "Effect of Rotation on Temperature Response of Thermochromic Liquid Crystal," Int. J. Heat Fluid Flow, **17**, pp. 491–499.

[9] Camci, C., Glezer, B., Owen, J. M., Pilbrow, R. G., and Syson, B. J., 1996, "Application of Thermochromic Liquid Crystal to Rotating Surfaces," ASME J. Turbomach., **118**, pp. 408–413.

[10] Gillespie, D. R. H., Wang, Z., and Ireland, P. T., 1998, "Full Surface Local Heat Transfer Coefficient Measurements in a Model of an Integrally Cast Impingement Cooling Geometry," ASME J. Turbomach., **120**, pp. 92–99.

[11] Newton, P. J., Yan, Y., Stevens, N. E., Evatt, S. T., Lock, G. D., and Owen, J. M., 2003, "Transient Heat Transfer Measurements Using Thermochromic Liquid Crystal. Part 1: An Improved Technique," Int. J. Heat Fluid Flow, **24**, pp. 14–22.

[12] Yan, Y., and Owen, J. M., 2002, "Uncertainties in Transient Heat Transfer Measurements With Liquid Crystal," Int. J. Heat Fluid Flow, **23**, pp. 29–35.

[13] Owen, J. M., Newton, P. J., and Lock, G. D., 2003, "Transient Heat Transfer Measurements Using Thermochromic Liquid Crystal. Part 2: Experimental Uncertainties," Int. J. Heat Fluid Flow, **24**, pp. 23–28.

[14] Chen, J.-X., Gan, X., and Owen, J. M., 1996, "Heat Transfer in an Air-Cooled Rotor-Stator System," ASME J. Turbomach., **118**, pp. 444–451.

[15] Butler, R. J., and Baughn, J. W., 1996, "The Effect of the Thermal Boundary Condition on Transient Method Heat Transfer Measurements on a Flat Plate With a Laminar Boundary Layer," ASME J. Heat Transfer, **118**, pp. 831–837.

[16] Lin, M., and Wang, T., 2002, "A Transient Liquid Crystal Method Using a 3-D Inverse Transient Conduction Scheme," Int. J. Heat Mass Transfer, **45**, pp. 3491–3501.